Journal of Power Sources 196 (2011) 10322–10327

Contents lists available at ScienceDirect

Journal of Power Sources

journal homepage: www.elsevier.com/locate/jpowsour

Structural and thermal stabilities of layered $Li(Ni_{1/3}Co_{1/3}Mn_{1/3})O_2$ materials in 18650 high power batteries

Yan-Bing He[a,b], Feng Ning[a,c], Quan-Hong Yang[a,b], Quan-Sheng Song[b], Baohua Li[a,*], Fangyuan Su[b], Hongda Du[a], Zhi-Yuan Tang[b], Feiyu Kang[a,c]

[a] Key Laboratory of Thermal Management Engineering and Materials, Graduate School at Shenzhen, Tsinghua University, Shenzhen 518055, China
[b] Department of Applied Chemistry, School of Chemical Engineering and Technology, Tianjin University, Tianjin 300072, China
[c] Laboratory of Advanced Materials, Department of Materials Science and Engineering, Tsinghua University, Beijing 100084, China

ARTICLE INFO

Article history:
Received 9 June 2011
Received in revised form 8 August 2011
Accepted 9 August 2011
Available online 12 August 2011

Keywords:
Layered lithium nickel cobalt manganese oxides
High power batteries
Stability
Abusive conditions

ABSTRACT

The structural and thermal stabilities of the layered $Li(Ni_{1/3}Co_{1/3}Mn_{1/3})O_2$ cathode materials under high rate cycling and abusive conditions are investigated using the commercial 18650 $Li(Ni_{1/3}Co_{1/3}Mn_{1/3})O_2$/graphite high power batteries. The $Li(Ni_{1/3}Co_{1/3}Mn_{1/3})O_2$ materials maintain their layered structure even when the power batteries are subjected to 200 cycles with 10 C discharge rate at temperatures of 25 and 50 °C, whereas their microstructure undergoes obvious distortion, which leads to the relatively poor cycling performance of power batteries at high charge/discharge rates and working temperature. Under abusive conditions, the increase in the battery temperature during overcharge is attributed to both the reactions of electrolyte solvents with overcharged graphite anode and $Li(Ni_{1/3}Co_{1/3}Mn_{1/3})O_2$ cathode and the Joule heat that results from the great increase in the total resistance (R_{cell}) of batteries. The reactions of fully charged $Li(Ni_{1/3}Co_{1/3}Mn_{1/3})O_2$ cathodes and graphite anodes with electrolyte cannot be activated during short current test in the fully charged batteries. However, these reactions occur at around 140 °C in the fully charged batteries during oven test, which is much lower than the temperature of about 240 °C required for the reactions outside batteries.

1. Introduction

Layered $Li(Ni_{1/3}Co_{1/3}Mn_{1/3})O_2$ materials, with a theoretical capacity of 278 mAh g^{-1}, possess specific capacity of 150 mAh g^{-1} within the voltage range of 2.5–4.2 V, which is higher than that of $LiCoO_2$ materials. In addition, the layered $Li(Ni_{1/3}Co_{1/3}Mn_{1/3})O_2$ materials show better thermal stability than $LiCoO_2$ and $Li(Ni_{0.8}Co_{0.15}Al_{0.05})O_2$ materials [1–4]. Liu et al. [5] reported that the batteries using the mixture of $Li(Ni_{1/3}Co_{1/3}Mn_{1/3})O_2$ and $LiCoO_2$ as the cathode materials showed better safety performance than that of the $LiCoO_2$ batteries. The layered $Li(Ni_{1/3}Co_{1/3}Mn_{1/3})O_2$ materials with good electrochemical performance can be synthesized by various methods, such as solid-state reaction [6,7], hydroxide co-precipitation [8–10], sol–gel [11], spray-drying [12], and spray-microwave [13]. Therefore, the layered $Li(Ni_{1/3}Co_{1/3}Mn_{1/3})O_2$ materials are very promising for use as the positive electrode in lithium-ion high power batteries.

So far, the electrochemical performance of $Li(Ni_{1/3}Co_{1/3}Mn_{1/3})O_2$ materials has been mainly investigated using coin cells, and their thermal stability has been mainly analyzed by examining the reactivity of $Li(Ni_{1/3}Co_{1/3}Mn_{1/3})O_2$ materials with electrolyte at high temperatures using differential scanning calorimetry (DSC) and accelerating rate calorimetry (ARC) [1,14]. In fact, the reaction of $Li(Ni_{1/3}Co_{1/3}Mn_{1/3})O_2$ materials with electrolyte, which occurs at high temperatures inside batteries, is quite different with that outside batteries. The decomposition temperature of electrolyte on the fully charged $Li(Ni_{1/3}Co_{1/3}Mn_{1/3})O_2$ electrode inside batteries may be significantly lower than that outside batteries. Thus, it is very important to investigate the structural and thermal stabilities of $Li(Ni_{1/3}Co_{1/3}Mn_{1/3})O_2$ materials inside the power batteries.

In our previous work [15], we prepared commercial 18650 $Li(Ni_{1/3}Co_{1/3}Mn_{1/3})O_2$/graphite high power batteries using the synthesized $Li(Ni_{1/3}Co_{1/3}Mn_{1/3})O_2$ materials and investigated their electrochemical performance at 25 and 50 °C. It was found that the high power batteries showed excellent high rate discharge and cycling performance. In this paper, we further investigated the structural and thermal stability of $Li(Ni_{1/3}Co_{1/3}Mn_{1/3})O_2$ cathode materials under high rate cycling and abusive conditions in 18650 $Li(Ni_{1/3}Co_{1/3}Mn_{1/3})O_2$/graphite high power batteries. The structural stability of the $Li(Ni_{1/3}Co_{1/3}Mn_{1/3})O_2$ materials was analyzed after 200 cycles with different charge and discharge rate at 25 and 50 °C. The high power batteries were subjected to abusive tests,

* Corresponding author. Tel.: +86 755 26036419; fax: +86 755 26036419.
E-mail address: libh@mail.sz.tsinghua.edu.cn (B. Li).

0378-7753/$ – see front matter © 2011 Elsevier B.V. All rights reserved.
doi:10.1016/j.jpowsour.2011.08.042

including overcharge, short current and oven test to examine the thermal stability of $Li(Ni_{1/3}Co_{1/3}Mn_{1/3})O_2$ cathode materials in the electrolyte and reveal the heating mechanism of the commercial high power batteries.

2. Experimental

The layered $Li(Ni_{1/3}Co_{1/3}Mn_{1/3})O_2$ materials and 18650 $Li(Ni_{1/3}Co_{1/3}Mn_{1/3})O_2$/graphite high power batteries with a capacity of 1300 mAh were prepared using the same method as described in our previous report [15]. The cycling performance of batteries was examined between 2.75 and 4.20 V at temperatures of 25 and 50 °C with different charge and discharge rates. The fully discharged high power batteries before and after cycling were transferred to a glove box and then dissembled. The $Li(Ni_{1/3}Co_{1/3}Mn_{1/3})O_2$ cathode was rinsed using dimethyl carbonate (DMC) to remove the electrolyte from the cathode surface. Then, the $Li(Ni_{1/3}Co_{1/3}Mn_{1/3})O_2$ samples were taken from the cathode and dried in the glove box antechamber to remove the residual DMC. X-ray diffraction (XRD) patterns of the $Li(Ni_{1/3}Co_{1/3}Mn_{1/3})O_2$ samples before and after cycling were obtained by a PANAlytical X'Pert powder diffractometer using Co Kα radiation in an angular range of 15–90° (2θ) with a 0.02° (2θ) step. The structural parameters were calculated by using the MDI Jade 5.0 profile matching refinement method for the XRD diagrams.

The electrochemical working station (Gamry PCI 4–750) was used to measure the electrochemical impedance spectrum (EIS) of the 18650 $Li(Ni_{1/3}Co_{1/3}Mn_{1/3})O_2$/graphite high power batteries at fully discharged state before and after cycling. The $Li(Ni_{1/3}Co_{1/3}Mn_{1/3})O_2$ cathode was used as the working electrode, and the graphite anode as counter electrode. The impedance was measured by applying a 5 mV of ac oscillation with the frequency ranging from 100 kHz to 0.01 Hz.

The abusive tests of batteries included overcharge, short current and oven tests. The overcharge tests were conducted by further charging the batteries with a constant current of 1.3 A (1 C) using a 10 V power supply (1 C/10 V) after they were fully charged to 4.2 V. The short current tests were conducted by connecting the cathode tab with the anode tab using a low resistance lead (<5 mΩ) after the batteries were fully charged to 4.2 V. The oven tests were conducted in the way that the batteries were fully charged to 4.2 V and then laid in an oven, and the oven temperature was then raised from environment temperature and kept stable at 150 °C. A multimeter was also connected to the cathode and anode tab to measure the battery voltage in the short circuit and oven experiments. A type-K thermal couple was attached to the surface of batteries to record the temperature change during the abusive tests. The EIS of batteries before and after the overcharge test were measured.

3. Results and discussion

3.1. Structural stability of layered $Li(Ni_{1/3}Co_{1/3}Mn_{1/3})O_2$ materials during cycling

Structural stability of $Li(Ni_{1/3}Co_{1/3}Mn_{1/3})O_2$ materials during cycling at 25 °C was investigated by cycling the 18650 $Li(Ni_{1/3}Co_{1/3}Mn_{1/3})O_2$/graphite high power batteries for up to 200 times with charge rates of 1 and 5 C and discharge rate of 10 C at 25 °C. From Fig. 1a, the capacity of power batteries at the 200th cycle is found to be 1161.03 and 1095.76 mAh for the charge rate of 1 and 5 C, which corresponds to the capacity retention of 92.94 and 88.32%, respectively. This indicates that the high power batteries show excellent high rate cycling performance, which slightly deteriorates at a high charge rate of 5 C.

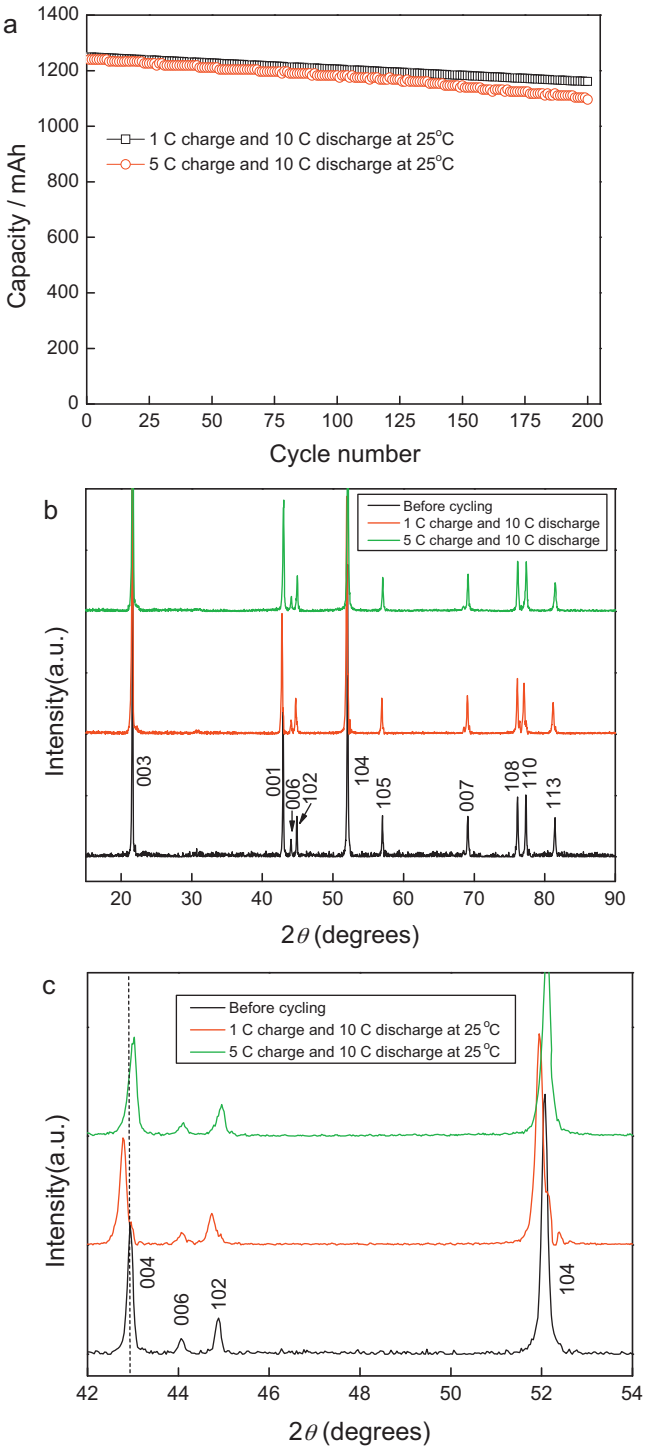

Fig. 1. Cycling performance of 18650 $Li(Ni_{1/3}Co_{1/3}Mn_{1/3})O_2$/graphite high power batteries with charge rates of 1 and 5 C and discharge rate of 10 C at 25 °C (a), XRD patterns of $Li(Ni_{1/3}Co_{1/3}Mn_{1/3})O_2$ materials before and after 200 cycles at 25 °C within the 2θ angles in the range of 15–90° (b) and 42–54° (c).

XRD patterns of $Li(Ni_{1/3}Co_{1/3}Mn_{1/3})O_2$ materials before and after cycling at fully discharged state are shown in Fig. 1b. It can be seen that the $Li(Ni_{1/3}Co_{1/3}Mn_{1/3})O_2$ materials maintain their layered structure even having been subjected to 200 cycles with charge rate of 5 C and discharge rate of 10 C. From Fig. 1c, it can be seen that the XRD peaks of $Li(Ni_{1/3}Co_{1/3}Mn_{1/3})O_2$ cycled with charge rate of 1 C are shifted toward the lower 2θ angles, while the XRD peaks of $Li(Ni_{1/3}Co_{1/3}Mn_{1/3})O_2$ cycled with charge rate of 5 C

Table 1
Lattice constants of fully discharged $Li(Ni_{1/3}Co_{1/3}Mn_{1/3})O_2$ materials before and after cycling at 25 °C.

Lattice constant	a (Å)	c (Å)
Before cycling	2.8624	14.3125
200 cycles with 1 C charge and 10 C discharge at 25 °C	2.8685	14.3242
200 cycles with 5 C charge and 10 C discharge at 25 °C	2.8648	14.2769

are shifted toward the higher 2θ angles. In addition, the XRD peaks of $Li(Ni_{1/3}Co_{1/3}Mn_{1/3})O_2$ after cycling become wider as compared with those of the material before cycling. Table 1 shows the lattice constant of $Li(Ni_{1/3}Co_{1/3}Mn_{1/3})O_2$ before and after cycling. It can be seen that the parameter a slightly increases for both charge rates of 1 and 5 C. The parameter c has a slight increase for the charge rate of 1 C and an obvious decrease for the charge rate of 5 C. Thus, for $Li(Ni_{1/3}Co_{1/3}Mn_{1/3})O_2$ cycled with charge rate of 1 C and discharge rate of 10 C, the slight increase in parameters a and c leads to the shift of XRD peaks to lower 2θ angles and the crystal expansion of the material. For $Li(Ni_{1/3}Co_{1/3}Mn_{1/3})O_2$ cycled with charge rate of 5 C and discharge rate of 10 C, the obvious decrease in parameter c results in the shift of XRD peaks to higher 2θ angles and the crystal shrinkage of the material. This indicates that the microstructure of $Li(Ni_{1/3}Co_{1/3}Mn_{1/3})O_2$ materials undergoes some distortion during cycling with high charge and discharge rates at 25 °C.

It is easily understood that the crystal expansion of $Li(Ni_{1/3}Co_{1/3}Mn_{1/3})O_2$ after cycling is due to the structural fatigue caused by repeated contraction and expansion during cycling and the temperature increase resulted from the high discharge current. But the crystal shrinkage is also observed for $Li(Ni_{1/3}Co_{1/3}Mn_{1/3})O_2$ after cycling with high charge rate of 5 C and discharge rate of 10 C. The obvious decrease in parameter c suggests a decrease in the layers distance of oxygen, Li and ordered Ni–Mn–Co. When the batteries are charged at a high current, the $Li(Ni_{1/3}Co_{1/3}Mn_{1/3})O_2$ electrodes are in an environment of high polarization and Li ions are pulled out rapidly from the interior of $Li(Ni_{1/3}Co_{1/3}Mn_{1/3})O_2$. This may induce a slight collapse of the layered structure of $Li(Ni_{1/3}Co_{1/3}Mn_{1/3})O_2$ materials after they are subjected to many times of charging with high current, which can result in the decrease of the parameter c. In addition, the Ni and Mn ions may also be depleted from the interior of $Li(Ni_{1/3}Co_{1/3}Mn_{1/3})O_2$ at high polarization during charging. The relatively poor cycling performance of the batteries at high charge rate may be partly attributed to the slight collapse of the microstructure of $Li(Ni_{1/3}Co_{1/3}Mn_{1/3})O_2$ materials during cycling.

The high power batteries were cycled 200 times with charge rate of 1 C and discharge rates of 5 and 10 C at 50 °C to investigate the structural stability of $Li(Ni_{1/3}Co_{1/3}Mn_{1/3})O_2$ during cycling. Fig. 2a shows that the capacity retention of power batteries is 87.73 and 75.89% for the discharge rate of 5 and 10 C, respectively. It can be seen that the power batteries show inferior cycling performance at 50 °C as compared with that at 25 °C. XRD patterns in Fig. 2b indicate that the $Li(Ni_{1/3}Co_{1/3}Mn_{1/3})O_2$ materials also maintain their layered structure after 200 cycles with discharge rates of 5 and 10 C at 50 °C. However, the XRD peaks of $Li(Ni_{1/3}Co_{1/3}Mn_{1/3})O_2$ after cycling become wider and the XRD peaks for the discharge rate of 10 C are shifted toward lower 2θ angles. From the lattice constant in Table 2, it can be seen that the parameter a has little change after

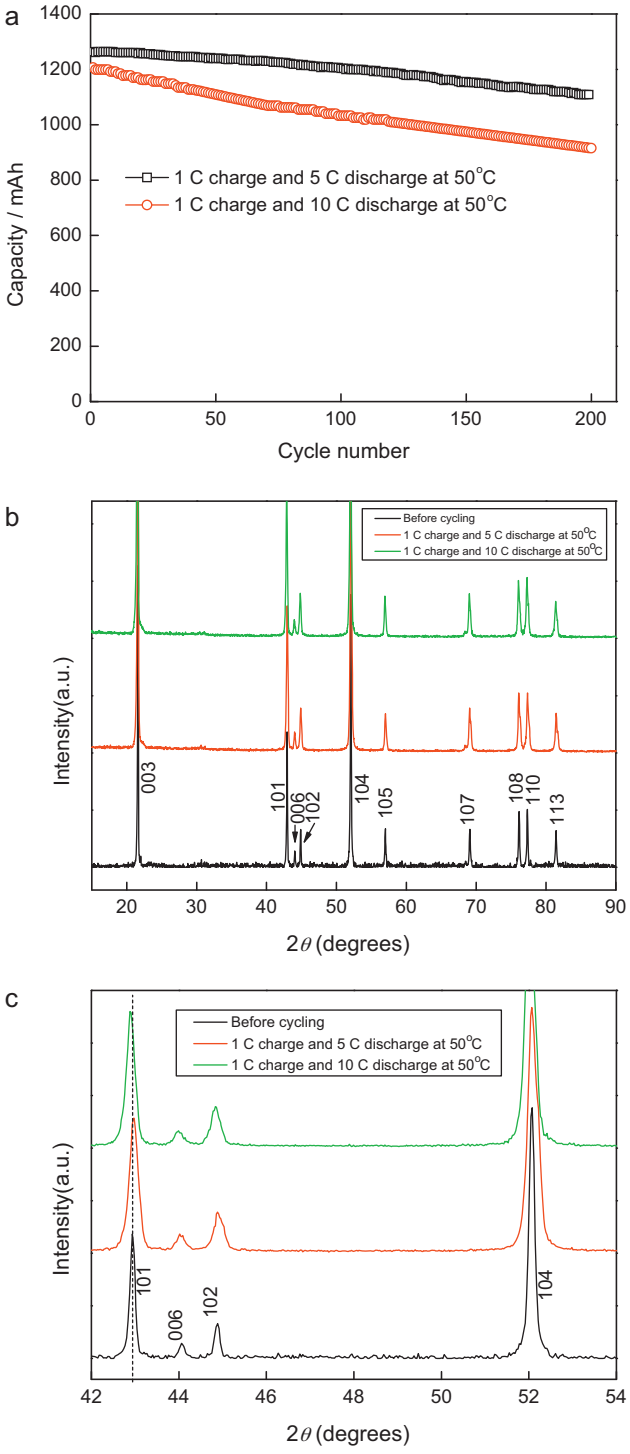

Fig. 2. Cycling performance of 18650 $Li(Ni_{1/3}Co_{1/3}Mn_{1/3})O_2$/graphite high power batteries with charge rate of 1 C and discharge rates of 5 and 10 C at 50 °C (a), XRD patterns of $Li(Ni_{1/3}Co_{1/3}Mn_{1/3})O_2$ materials before and after 200 cycles at 50 °C within the 2θ angles in the range of 15–90° (b) and 42–54° (c).

Table 2
Lattice constants of fully discharged $Li(Ni_{1/3}Co_{1/3}Mn_{1/3})O_2$ materials before and after cycling at 50 °C.

Lattice constant	a (Å)	c (Å)
Before cycling	2.8624	14.3125
200 cycles with 1 C charge and 5 C discharge at 50 °C	2.8626	14.3247
200 cycles with 1 C charge and 10 C discharge at 50 °C	2.8617	14.3571

200 cycles, whereas the parameter c increases obviously with the increase in the discharge rate, which results in the widening and shift of XRD peaks. In addition, for $Li(Ni_{1/3}Co_{1/3}Mn_{1/3})O_2$ cycled with charge rate of 1 C and discharge rate of 10 C, it can be seen that the parameter c increases greatly with the increase in working temperature, which suggests an increase in the layers distance of oxygen, Li and ordered Ni–Mn–Co. It is well-known that the delithiation of $Li(Ni_{1/3}Co_{1/3}Mn_{1/3})O_2$ leads to an expansion in the

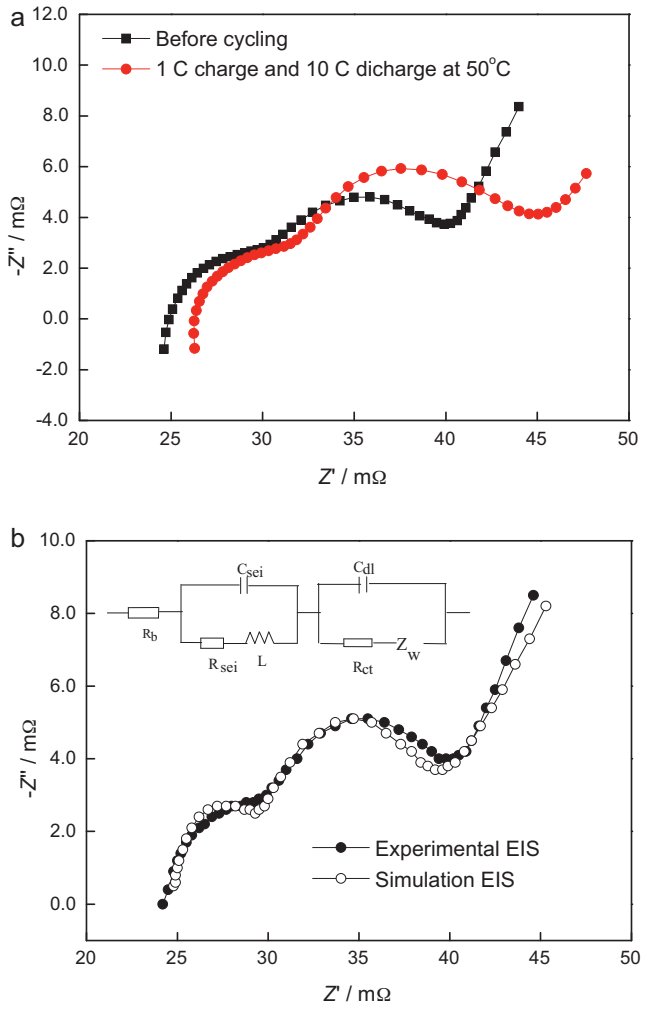

Fig. 3. EIS of 18650 $Li(Ni_{1/3}Co_{1/3}Mn_{1/3})O_2$/graphite high power batteries at fully discharged state before and after 200 cycles with charge rate of 1 C and discharge rate of 10 C at 50 °C (a), the experimental and simulation EIS data of 18650 high power batteries before cycling and the equivalent circuit used to fit the EIS (b).

parameter *c* due to the increase of the repulsive force between the oxygen layers [15]. In this work, the batteries are fully discharged before disassembling. Thus, the relatively large value of parameter *c* indicates that the fully discharged $Li(Ni_{1/3}Co_{1/3}Mn_{1/3})O_2$ materials subjected to 200 cycles with discharge rate of 10 C at 50 °C contain small amount of lithium ions, suggesting that the lithiation performance of $Li(Ni_{1/3}Co_{1/3}Mn_{1/3})O_2$ becomes deteriorated after cycling at high temperature.

The EIS of 18650 $Li(Ni_{1/3}Co_{1/3}Mn_{1/3})O_2$/graphite high power batteries at fully discharged state before and after 200 cycles with 1 C charge and 10 C discharge at 50 °C are plotted in Fig. 3a. Fig. 3b also shows the EIS which were simulated by ZSimpWin 3.0 software using the equivalent circuit. According to the equivalent circuit, the EIS are composed of two partially overlapped semicircles at high to middle frequency and a straight slope line at low frequency end. Table 3 shows the individual values of the bulk resistance (R_b), resistance of the solid electrolyte interface (R_{sei}), and charge-transfer resistance (R_{ct}). It can be seen that the R_b increases after cycling due to the consumption of electolyte at high temperature. However, there is no significant increase observed for the R_{sei} after cycling. The change in R_{sei} observed in a Li-ion battery can be ascribed to the combined effect of two reverse changes in the respective R_{sei} value of the graphite anode and $Li(Ni_{1/3}Co_{1/3}Mn_{1/3})O_2$ cathode [16,17]. The R_{sei} of $Li(Ni_{1/3}Co_{1/3}Mn_{1/3})O_2$ cathode is much larger than that of the graphite anode when the $Li(Ni_{1/3}Co_{1/3}Mn_{1/3})O_2$/graphite batteries are at fully discharged state [16]. This suggests that more SEI formation on the graphite due to the instable electrolyte at high temperature may lead to an obvious increase in R_{sei} of graphite anode, which does not result in a great increase in R_{sei} of fully discharged $Li(Ni_{1/3}Co_{1/3}Mn_{1/3})O_2$/graphite batteries. However, it can be seen that the R_{ct} of the batteries after cycling shows a greater increase than the R_{sei}, which can be attributed to the microstructure distortion of $Li(Ni_{1/3}Co_{1/3}Mn_{1/3})O_2$ materials during cycling at high temperature. Thus, the consumption of electrolyte and the microstructure distortion of $Li(Ni_{1/3}Co_{1/3}Mn_{1/3})O_2$ materials result in the relatively poor cycling performance of batteries at high temperature.

Table 3
Values of the R_b, R_{sei} and R_{ct} obtained by simulating the data of Fig. 3a.

Resistance	R_b (mΩ)	R_{sei} (mΩ)	R_{ct} (mΩ)
Before cycling	24.12	5.46	7.82
200 cycles with 1 C charge and 10 C discharge at 50 °C	26.04	5.73	10.44

3.2. *Thermal stability of layered $Li(Ni_{1/3}Co_{1/3}Mn_{1/3})O_2$ materials under abusive conditions*

18650 $Li(Ni_{1/3}Co_{1/3}Mn_{1/3})O_2$/graphite high power batteries were overcharged by 1 C/10 V to investigate the thermal stability and reveal the heating mechanism of the batteries. It can be seen from Fig. 4a that the $Li(Ni_{1/3}Co_{1/3}Mn_{1/3})O_2$/graphite high power batteries show similar overcharge characteristics with those of the $LiCoO_2$/graphite batteries [18–20]. The battery voltage increases gradually during the overcharge. The battery temperature starts to increase when the batteries are overcharged to 4.6 V. At this stage, the exothermic reactions, such as the electrolyte decomposition, the reaction between the delithiated cathode and the electrolyte, and the violent reaction between the overcharged anode and the electrolyte do not occur.

The EIS of high power batteries at 4.2 (before overcharge) and 4.8 V (after overcharge) are plotted in Fig. 4b. It can be seen that the total resistance R_{cell}, which is composed of R_b, R_{sei} and R_{ct}, increases greatly after overcharge due to the significant increase in R_{sei} and R_{ct}. Fig. 4a shows that the battery voltage increases from 4.2 to 4.8 V after the batteries are overcharged for about 30 min. At this stage, the delithiation of overcharged $Li(Ni_{1/3}Co_{1/3}Mn_{1/3})O_2$ materials becomes very difficult due to a much lower lithium ion concentration in the overcharged $Li(Ni_{1/3}Co_{1/3}Mn_{1/3})O_2$ materials, which results in the great increase in the electrochemical reaction resistance. In addition, the lithium ions cannot be inserted into the fully lithiated graphite anode and they will be deposited on the surface of graphite anode to form lithium metal, which leads to the great increase of R_{sei}. Our previous work also showed that the R_{cell} increased significantly with increases of 80 to 100% in the state of charge (SOC) [15]. The increase of R_{cell} makes the batteries generate some Joule heat during overcharge, which can be described as $Q = i^2 R_{cell} t$, where Q represents the heat generated, i is charge current and t is overcharge time. However, the heat dissipation also occurs during the battery overcharge, which is related to the size and shape of batteries. If the heat generation and dissipation are in balance, the battery temperature will not change. This occurs only when the batteries are overcharged to below 4.6 V. When the batteries are overcharged to above 4.6 V and the rate of heat generation is higher than that of heat dissipation, this balance will be broken and the battery temperature will rise. Thus, the increase in the battery temperature

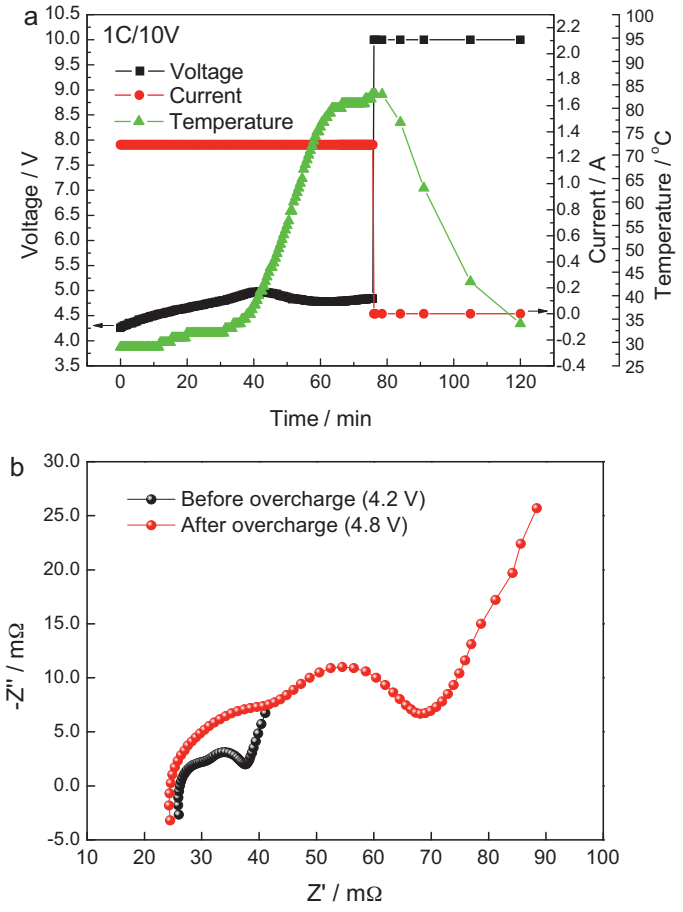

Fig. 4. Voltage, current and temperature profiles of 18650 $Li(Ni_{1/3}Co_{1/3}Mn_{1/3})O_2$/graphite high power batteries during 1 C/10 V overcharge test (a); EIS of high power batteries at 4.2 (before overcharge) and 4.8 V (after overcharge) (b).

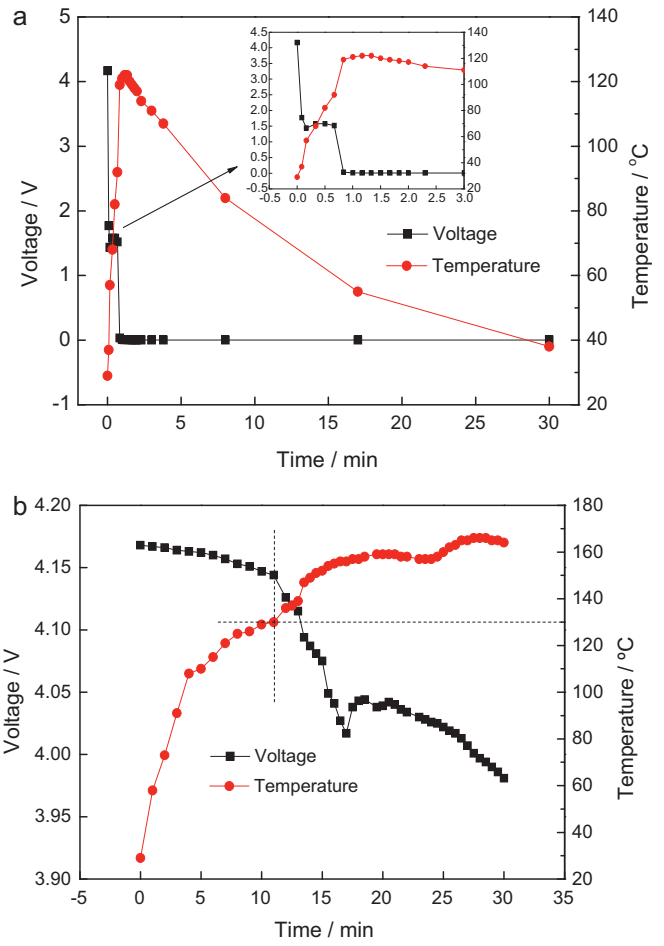

Fig. 5. Voltage and temperature profiles of fully charged 18650 $Li(Ni_{1/3}Co_{1/3}Mn_{1/3})O_2$/graphite batteries during short current (a) and oven test at 150 °C (b).

during overcharge from 4.6 to 4.8 V is attributed to the Joule heat which is generated from the great increase of R_{cell}.

The battery temperature goes up quickly when the battery voltage reaches 4.90 V. It also can be observed from Fig. 4a that the voltage shows some complicated changes, where it increases slowly from 4.90 to 4.97 V and subsequently shows a short plateau for about 5 min, then decreases gradually to 4.78 V and increases again. The voltage change starting at 4.9 V (*i.e.* in the period from about 40 to 80 min) is a typical symbol of electrolyte decomposition, caused by reactions of electrolyte solvents with overcharged anode and cathode, respectively. Study results have shown that the SEI decomposition reaction occurs at around 120 °C and the main exothermic reactions of the lithiated graphite with solvents outside the battery occur at above 240 °C [21–23]. In addition, the violent reactions between the overcharged anode (with deposited lithium) and the electrolyte solvents at high temperature are activated by the rapid exothermic reaction of the delithiated cathode and the electrolyte [19]. Therefore, when the batteries are overcharged to 4.9 V, the electrolyte is first oxidized on the overcharged $Li(Ni_{1/3}Co_{1/3}Mn_{1/3})O_2$ cathode and the reaction between the electrolyte and overcharged cathode generates much gases and heat [19]. Moreover, the reaction consumes overcharge current. When the battery voltage reaches 4.97 V, the amount of the charge consumed by the reaction of the electrolyte and overcharged cathode is equal to that supplied by the overcharge. Thus, the voltage of the overcharged batteries shows a short plateau at the overcharging time of 39–44 min. The reaction rate of the overcharged cathode and electrolyte will increase along with the rise of the battery temperature, and the reactions of overcharged graphite anode (with deposited lithium) and the electrolyte solvents are also activated. In this period most of the applied electric energies are converted to heat, resulting in a rapid increase in the temperature. When the charge consumption exceeds the charge supply from overcharge, and where the anode and cathode materials are destroyed severely, the battery voltage would gradually decrease. The quantity of the electrolyte gradually decreases with the electrolyte decomposition. The amount of the charge consumed by the electrolyte decomposition is less than that supplied by the overcharge, which leads to the rise of the battery voltage again. Meanwhile, gases are produced in the overcharge reactions, which make the pressure inside the battery build up quickly, and then the overcharge current falls to zero because the battery vents works and the battery loses most of electrolytes, which results in the failure of passing any currents across the battery. In this case, the batteries cannot be charged again, which ensures no explosion of the batteries. In the overcharge process, the battery temperature increases to about 84 °C, which is attributed to the heat generated from the exothermic reactions of electrolyte solvents with overcharged anode and cathode and the Joule heat generated from the great increase of the total resistance (R_{cell}) of batteries.

The short current testing is similar to the huge current discharge testing. It can be seen from Fig. 5a that the voltage decreases to about 1.5 V and subsequently shows a short plateau, and then rapidly decreases to 0 V. The battery temperature rises greatly to the maximum value of about 120 °C. The batteries are heated

much rapidly by the irreversible heat generation from the current passing through the electrodes. This rapid heating process produces a steep temperature profile with the highest temperature at the battery core. It can be seen that the batteries are not runaway and the battery temperature starts to decrease at the end of discharge plateau. Thus, the reactions of the $Li(Ni_{1/3}Co_{1/3}Mn_{1/3})O_2$ cathode and graphite anode with the electrolyte cannot be activated during the short current test of the batteries. However, the SEI film on the graphite anode may be destroyed.

For the oven test, it can be observed from Fig. 5b that the voltage of fully charged batteries decreases gradually with the increase in the battery temperature, which indicates that the self-discharge of batteries becomes significant at high temperature. When the battery temperature increases to around 130 °C, the battery voltage decreases quickly, which is mainly attributed to the SEI decomposition. The maximum value of the battery temperature during oven test reaches 166 °C, which is much higher than the oven temperature of 150 °C. In fact, the energy released from the SEI decomposition is low and is not enough to lead to a great increase in the battery temperature [24]. Fig. 5b also indicates that the battery temperature increases greatly and the battery voltage decreases rapidly when the battery temperature reaches 140 °C. The separator of polyethylene membrane may shrink when the battery temperature is higher than 140 °C, which may lead to physical contact (circuit shorting) of cathode and anode. From Fig. 5a, it is seen that the battery voltage decreases rapidly to about 0 V within 1 min when the battery is under fully short current. Whereas, Fig. 5b shows that the battery voltage decreases from 4.17 to 3.98 V during 30 min oven test, which suggests that the fully short current of battery does not occur, and only micro-circuit shorting may occur during oven test due to the separator shrinkage or partial/local melting. The micro-circuit shorting does not generate much heat, which can not make the battery temperature increase greatly. This suggests that the reactions of the lithiated graphite anode and delithiated $Li(Ni_{1/3}Co_{1/3}Mn_{1/3})O_2$ cathode with the electrolyte take place at around 140 °C in the fully charged batteries, and the battery voltage is about 4.12 V at this point, which make the battery temperature exceed 150 °C. Thus, the reactivity of the delithiated $Li(Ni_{1/3}Co_{1/3}Mn_{1/3})O_2$ cathode and lithiated graphite anode with the electrolyte depends on whether the reactions are inside or outside batteries, and can be very different under these two situations. The reactions of the $Li(Ni_{1/3}Co_{1/3}Mn_{1/3})O_2$ cathode and graphite anode with the electrolyte inside batteries can be activated by the thermal and electric potential energies. Therefore, the temperature required for the reactions inside batteries is much lower than the temperature of about 240 °C required for the reactions outside batteries. The results in this work also indicate that the 18650 $Li(Ni_{1/3}Co_{1/3}Mn_{1/3})O_2$/graphite high power batteries do not explode during oven test at 150 °C, showing good safety performance.

4. Conclusions

The $Li(Ni_{1/3}Co_{1/3}Mn_{1/3})O_2$ materials maintain their layered structure even after 200 cycles with 10 C discharge rate at 25 and 50 °C, respectively. The microstructure of $Li(Ni_{1/3}Co_{1/3}Mn_{1/3})O_2$ has some kind of distortion, especially for the material subjected to cycling with high charge rate and high working temperature. During overcharge process, the electrolyte is oxidized on the $Li(Ni_{1/3}Co_{1/3}Mn_{1/3})O_2$ electrode when the battery voltage increases to 4.9 V, and the reactions of overcharge graphite anode with electrolyte are activated, and moreover, the total resistance (R_{cell}) of battery also increases greatly, which result in the rapid increase in the battery temperature. The fully charged battery is heated much rapidly to 120 °C by the irreversible heat generation from the current passing through the electrodes during short current test, which can not activate the reactions of the $Li(Ni_{1/3}Co_{1/3}Mn_{1/3})O_2$ cathode and graphite anode with the electrolyte. However, these reactions occur at around 140 °C inside the fully charged battery during oven test, which is much lower than the temperature of about 240 °C required for the reactions outside the battery. The fact that the reactions inside the battery can be activated by the thermal and electric potential energies makes the reactions occur easily inside the battery.

Acknowledgements

This work was supported by China Postdoctoral Science Foundation (No. 20100470296), Dongguan McNair Technology Co., Ltd., China, National Natural Science Foundation of China (No. 50802049 & No. 50632040), Shenzhen Technical Plan Project (No. JP200806230010A & No. SG200810150054A), Guangdong Province Innovation R&D Team Plan for Energy and Environmental Materials.

References

[1] Y. Wang, J. Jiang, J.R. Dahn, Electrochem. Commun. 9 (2007) 2534.
[2] J. Jiang, J.R. Dahn, Electrochem. Commun. 6 (2004) 39.
[3] D.D. MacNeil, J.R. Dahna, J. Electrochem. Soc. 148 (2001) A1205.
[4] D.D. MacNeil, J.R. Dahn, J. Electrochem. Soc. 149 (2002) A912.
[5] X. Liu, G. Zhu, K. Yang, J. Wang, J. Power Sources 174 (2007) 1126.
[6] J. Liu, W. Qiu, L. Yu, G. Zhang, H. Zhao, T. Li, J. Power Sources 174 (2007) 701.
[7] M. Kageyama, D. Li, K. Kobayakawa, Y. Sato, Y.-S. Lee, J. Power Sources 157 (2006) 494.
[8] S. Zhang, Electrochim. Acta 52 (2007) 7337.
[9] C. Deng, L. Liu, W. Zhou, K. Sun, D. Sun, Electrochim. Acta 53 (2008) 2441.
[10] C. Deng, S. Zhang, B.L. Fu, S.Y. Yang, L. Ma, J. Alloys Compd. 496 (2010) 521.
[11] W. Zhang, H. Liu, C. Hu, X. Zhu, Y. Li, Rare Metals 27 (2008) 158.
[12] Y. Li, C. Wan, Y. Wu, C. Jiang, Y. Zhu, J. Power Sources 85 (2000) 294.
[13] H.-Y. Chang, C.-I. Sheu, S.-Y. Cheng, H.-C. Wu, Z.-Z. Guo, J. Power Sources 174 (2007) 985.
[14] I. Belharouak, W. Lu, J. Liu, D. Vissers, K. Amine, J. Power Sources 174 (2007) 905.
[15] Y.B. He, Z.Y. Tang, Q.S. Song, H. Xie, Q.H. Yang, Y.G. Liu, G.W. Ling, J. Power Sources 185 (2008) 526.
[16] S.S. Zhang, K. Xu, T.R. Jow, Electrochim. Acta 49 (2004) 1057.
[17] S.S. Zhang, K. Xu, T.R. Jow, J. Power Sources 160 (2006) 1403.
[18] Y. Zeng, K. Wu, D. Wang, Z. Wang, L. Chen, J. Power Sources 160 (2006) 1302.
[19] T. Ohsaki, T. Kishi, T. Kuboki, N. Takami, N. Shimur, Y. Sato, M. Sekino, A. Satoh, J. Power Sources 146 (2005) 97.
[20] S. Hossain, Y.-K. Kim, Y. Saleh, R. Loutfy, J. Power Sources 161 (2006) 640.
[21] J. Jiang, J.R. Dahn, Electrochim. Acta 49 (2004) 4599.
[22] J.-i. Yamaki, H. Takatsuji, T. Kawamura, M. Egashira, Solid State Ionics 148 (2002) 241.
[23] I. Watanabe, J.-i. Yamaki, J. Power Sources 153 (2006) 402.
[24] R. Spotnitz, J. Franklin, J. Power Sources 113 (2003) 81.